ULTRA-WIDEBAND RADAR FOR BUILDING INTERIOR IMAGING

Traian Dogaru* and Calvin Le
U. S. Army Research Laboratory
Sensors and Electron Devices Directorate
Adelphi, Maryland 20783-1197

ABSTRACT

This paper presents both numeric simulations and radar measurements related to through the wall imaging technologies. We present synthetic aperture radar (SAR) images obtained by the Army Research Laboratory (ARL) Forward-Looking Radar system during field experiments and compare those with the results of our Xpatch computer models. We also demonstrate a computational approach based on the Finite Difference Time Domain (FDTD) algorithm in order to obtain the SAR images of a complex room. Our goals are both to validate the numerical simulations techniques and to understand the radar scattering phenomenology in this environment.

1. INTRODUCTION

In the modern battlefield environment, the requirement to counter asymmetric threats has resulted in a greatly increased likelihood that military ground forces will need to engage and neutralize hostile elements in an urban setting, where the enemy may be hiding in one of a number of buildings. In this scenario, the Future Force Warrior's situational awareness is often severely reduced, resulting in heightened personal danger and increased risk of collateral damage. Therefore, many defense agencies have demonstrated keen interest in developing Sensing Through the Wall (STTW) technologies. Among these, the low-frequency, ultra-wideband (UWB) microwave radar demonstrated great potential for building mapping, as well as for detecting targets behind walls. At the Army Research Laboratory (ARL), we have been actively involved in several major Department of Defense programs, developing computer models and algorithms in order to predict STTW system performance. Moreover, we demonstrated the capabilities of our in-house designed Synchronous Impulse Reconstruction (SIRE) radar (Ressler et al., 2007) for building imaging, as well as concealed human target detection, during field measurements. This paper describes the building imaging field experiments performed with the SIRE radar and compares the results with our Xpatch computer models. We also create synthetic aperture radar (SAR) images of a complex room based on Finite-Difference Time-Domain (FDTD) numeric simulations. These computer models evidence some interesting phenomenology effect specific to STTW environments and help us predict the operational performance of a STTW imaging radar.

2. SIRE RADAR MEASUREMENTS

2.1. Overview of the SIRE radar

The ARL SIRE radar is a vehicle-borne, UWB impulse-based system, designed to create SAR images in various configurations. The transmitters are commercial monocycle generators with pulse width of approximately 1 ns and a pulse repetition frequency (PRF) of 1 MHz. The total average power integrated across the bandwidth is only 5 mW in order to minimize the interference potential to other spectrum users. The transmitting antennas are transversal electro-magnetic (TEM) horns designed to match the pulse spectrum of this radar. Modeling studies have shown that a pair of transmitters situated at the two ends of the receive array provides the same cross range resolution as a monostatic configuration with an equal number of transmitters and receivers (Ressler et al., 2007). In terms of bandwidth, 90% of the transmitted energy lies between 300 – 2400 MHz. The receiver system employs a linear array of 16 identical receive Vivaldi notch antennas mounted in a 2 m wide platform, which provides a real aperture when the radar operates in a stationary mode. When operating in a stripmap SAR mode, using data from multiple receive channels increases the signal-to-noise ratio, and enables detection of moving targets based on change detection. Each receiving antenna feeds its own base-band receiver/digitizer that integrate the data before sending it to the personal computer (PC) based operator's console display. This design is extensible to allow growth in the number of receive channels, improvement in integrated circuit performance and flexible upgrades in the firmware/software. In-depth detail of the SIRE radar system can be found in (Ressler et al., 2007).

Report Documentation Page

Form Approved
OMB No. 0704-0188

1. REPORT DATE	2. REPORT TYPE	3. DATES COVERED
01 DEC 2008	**N/A**	**-**

4. TITLE AND SUBTITLE	5a. CONTRACT NUMBER
Ultra-wideband Radar for Building Interior Imaging	5b. GRANT NUMBER
	5c. PROGRAM ELEMENT NUMBER
6. AUTHOR(S)	5d. PROJECT NUMBER
	5e. TASK NUMBER
	5f. WORK UNIT NUMBER
7. PERFORMING ORGANIZATION NAME(S) AND ADDRESS(ES) **U. S. Army Research Laboratory Sensors and Electron Devices Directorate Adelphi, Maryland 20783-1197**	8. PERFORMING ORGANIZATION REPORT NUMBER
9. SPONSORING/MONITORING AGENCY NAME(S) AND ADDRESS(ES)	10. SPONSOR/MONITOR'S ACRONYM(S)
	11. SPONSOR/MONITOR'S REPORT NUMBER(S)

12. DISTRIBUTION/AVAILABILITY STATEMENT
Approved for public release, distribution unlimited

13. SUPPLEMENTARY NOTES
See also ADM002187. Proceedings of the Army Science Conference (26th) Held in Orlando, Florida on 1-4 December 2008, The original document contains color images.

14. ABSTRACT

15. SUBJECT TERMS

16. SECURITY CLASSIFICATION OF:			17. LIMITATION OF ABSTRACT	18. NUMBER OF PAGES	19a. NAME OF RESPONSIBLE PERSON
a. REPORT	b. ABSTRACT	c. THIS PAGE			
unclassified	**unclassified**	**unclassified**	**UU**	**8**	

ARL has developed a suite of algorithms to process the SIRE radar data in the side looking mode. There are three main steps in forming the SAR image from the raw data: motion data processing, signal processing, and back-projection image formation. The motion compensation is based on GPS data from the rover and base station that are differentially post processed to provide the radar coordinates with centimeter accuracy as the vehicle is in motion. The purpose of the signal processing stage is to correct several artifacts such as the self-interference or the RF circuit-antenna mismatch in the transmitter chain. After these artifact removal procedures, the radar signal is filtered down to a frequency band of 300 – 1800 MHz, which is more favorable for STTW applications. Signal processing algorithms are then performed on the radar phase history data, and the back-projection image formation algorithm (Soumekh, 1999) is applied to produce a SAR image. We are using the true constant resolution back-projection algorithm (Nguyen and Sichina, 2007), in which every pixel within the SAR image is integrated using a different sub-aperture, in order to maintain a constant 60^0 integration angle. By this procedure we ensure a constant cross range resolution across the entire image.

2.2. Measurements setup

The one story abandoned barrack building structure displays a capital "H" layout in the horizontal plane, with bathrooms and showers located in the isle connecting the two living quarter rows. It has a large footprint of approximately 33 m by 27 m with a roof peak height of 4 m. The interior of the building is empty of furniture, but does have individual rooms separated by dividing walls that provide additional structure for imagery. The exterior of the building is covered with painted plywood siding, double hung windows, and asphalt roof shingled on a trusses wood roof frame. Most of the interior walls and the ceiling are covered with gypsum wall panels (drywalls). Cinder block walls are found in the bathroom/shower area. A view of the building, without the roof structure, is shown in Fig. 1.

The SIRE radar was repositioned from the forward looking mode to side-looking mode by simply rotating the radar platform bed by 90^0. In this side-looking configuration, the antennas system is aimed at a depression angle of approximately 11^0 (downward to the ground). The vehicle was driven at the speed of 1 m/s, along two sides of the building, while keeping a distance of approximately 10 m away from the exterior walls. It took about 90 seconds to acquire the radar data from both sides of the building. The down-range coverage of the SIRE radar extends between 8 and 33 m. The SAR images for each pass were independently formed and then incoherently combined in order to generate the overall building map.

3. COMPUTATIONAL APPROACHES

For the numerical part of this study we employ two widely used Computational Electromagnetics (CEM) modeling techniques, namely FDTD and ray-tracing combined with Physical Optics (PO). The FDTD code we used for this work is called AFDTD and was entirely developed at ARL for radar signature modeling. We ray-tracing code employed in our analysis is Xpatch, developed by Science Applications International Corporation (SAIC) under a grant from the U.S. Air Force.

The FDTD algorithm (Taflove, 1998) is based on discretizing Maxwell's time-domain equations, using finite differences in spatial and temporal dimensions. The computational space, with a uniform, rectangular, grid-like structure, is made of elementary cubic cells. The electromagnetic field components are computed along the cell's edges and faces, at discrete time steps. The FDTD algorithm is relatively simple to implement and parallelize, it can handle almost arbitrary media electric properties and geometries and can also provide results over a wide range of frequencies in one time-marching run. The major disadvantage of the FDTD technique is its computational cost, which scales up very rapidly with the physical size of the computational domain and the frequency of interest. Consequently, although FDTD is an exact solver capable of simulating a wide range of radar scenarios, there are certain bounds to the problem size that can be solved in a reasonable amount time with limited computer resources.

Xpatch is part of a family of CEM techniques that rely on high-frequency approximations to model field propagation and scattering. In particular, it implements ray tracing combined with PO to compute the radar return from arbitrary targets. In the applications presented here, the meshes describe the target surface, using a triangular facet model. Although Xpatch has been successfully used in a large number of radar applications, it has a number of limitations, which stem from the approximate nature of the methods it implements. However, as compared to FDTD, Xpatch can achieve vastly superior speed in modeling radar problems (typically 100 to 1000 times faster). In previous work (Dogaru and Le, 2008a), we have extensively validated the Xpatch code in the context of STTW modeling application, generally with very good results.

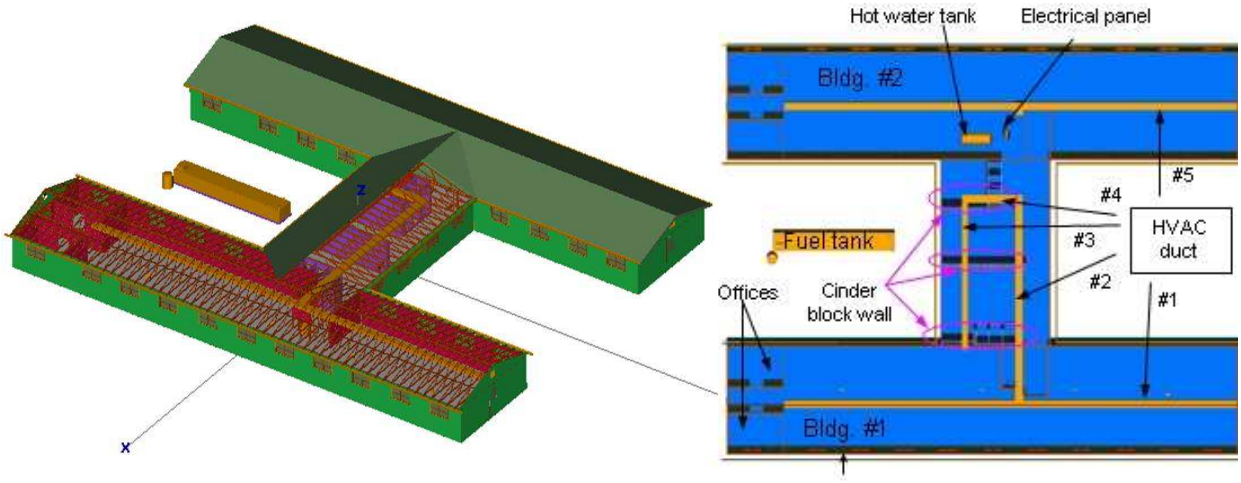

(a) (b)

Fig. 1. Barrack building layout showing: (a) perspective view; (b) top view with some construction details.

We have performed the simulations in this study at the U.S. Army Major Shared Resource Center (MSRC) on Linux Networx Evolocity II clusters. Note that the room modeling is the largest production run to date where we have used the AFDTD software. We employed the parallel version of this code, run on 24 processors for each different case or angle of incidence.

In all the following computer simulations, we assume that the radar operates as an UWB pulse radar. The radar transmitter and receiver are assumed to be in the far-field (we use plane-wave incident fields), at equal distance (regardless of incidence angle) to the phase reference, which is always placed in the middle of the room. The far-field operation is not necessarily a realistic assumption for a vehicle-based STTW radar (given the typically small standoff distance relative to the target size), but it is consistent with the image formation technique. In order to create the SAR images, we use the polar format algorithm algorithm (Soumekh, 1999), which converts the data in the frequency-angle domain from polar to rectangular coordinates and then takes an inverse two-dimensional Fast Fourier Transform (FFT). The images are presented as magnitude maps in dB scale. We use a Hanning window in both the frequency and the angular domain. The purpose of data windowing is to reduce the image sidelobes. However, by this procedure we also reduce the image resolution.

4. RESULTS

4.1. SAR images of the barrack building

Based on our site survey, we created a detailed Computer Aided Design (CAD) model of the APG barrack building, which was converted to a facet model comprising about 40,000 triangular facets as shown above in Fig. 1. A flat dielectric ground plane with the relative permittivity of $\varepsilon_r = 8$ is included in the model to represent the grassy area outside the building. Since the ground plane must be finite, while in the measurement setup the radar was placed at 10 m away from the front wall, we extended the dielectric ground plane 9 m beyond the building footprint (in all directions). Since some of the exterior wall internal structure was exposed, we were able to identify its geometry and materials. Two-by-four wooden studs (3.8 cm x 8.9 cm cross-section dimensions) are used for most exterior and interior walls, with some visible aluminum studs used in a few areas. Single and double cinder blocks wall structures are placed in the cross link building (shower/toilet area). Although we tried to include all the objects that were reasonable to mesh in our CAD model, some building features were not visible. Their placement was based on our educated guess. For example, the location of the aluminum heating-ventilation-air-conditioning (HVAC) ducts in the living quarters is based on the location of the ceiling duct vents, and their size is based on the HVAC ducts visible in the cross link building. Other objects were simply omitted from the mesh, because

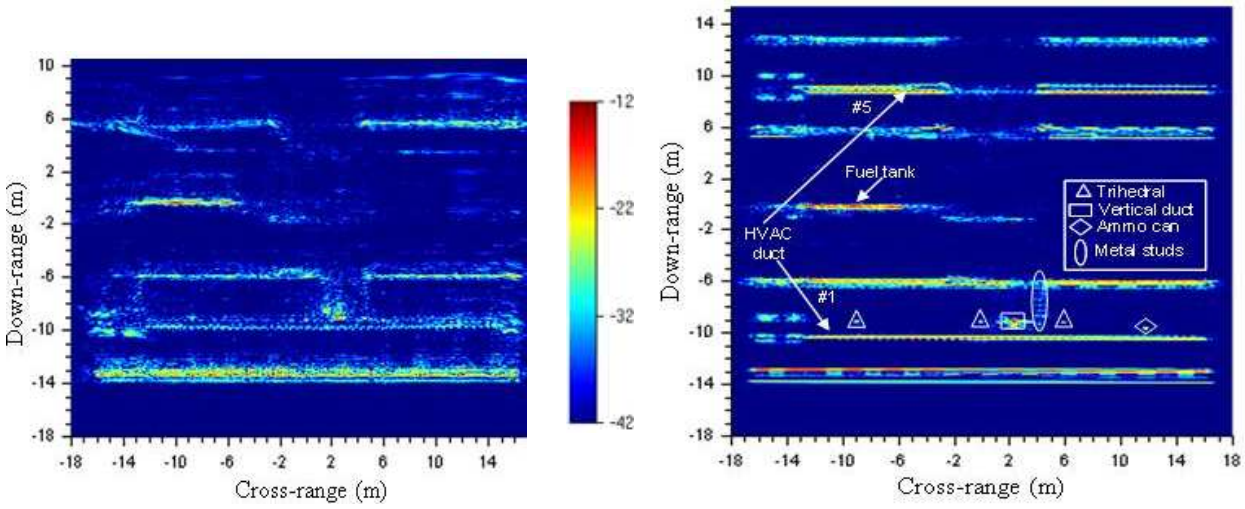

(a) (b)

Fig. 2. SAR images of the barrack building obtained along the radar path #1, showing (a) measured results and (b) simulated results.

they were too complicated to model or we were uncertain about their position and structure. Thus, we did not include the metal plumping pipes (mostly hidden behind the walls), small electrical conduits, insulations, and objects in an inaccessible area (boiler room).

Fig. 2 presents the measured SAR images obtained along the radar path #1 (a), and the simulated SAR images obtained for an aperture centered along a direction perpendicular to the long sides of the "H" (b). Since only the relative values of pixel intensities are important in comparing the images, we normalize each color map (in dB) to the maximum pixel intensity in the image. The absolute dB scales indicated for every figure are based on the Xpatch computed images. Importantly, we employ the same dynamic range for both the measured and simulated images. Notice that the SAR images obtained from Xpatch simulations display the entire down range building extent, while the measured image shows only part of that. This is an effect of the limited range swath of the SIRE radar. Otherwise, we notice a very good similarity between the two images in Figs. 2a and b.

In the Fig. 2b, the first long line (starting from the image bottom) is the scattering response from the aluminum gutter (part of the roof). Next is the return from the windows, followed closely by the strong scattering from the entire exterior wall. The barrack structure includes some small office rooms at the left end (two for each building, separated by a narrow hallway). The walls separating these rooms are also visible in the images. The gaps in these wall images are due to the missing doors. The long "zipper line" at the bottom of the image represents the HVAC duct #1. The zipper effect is due to the "blockage" by the wooden roof truss structure. All three calibration trihedral corners and the ammo can are visible in the simulated SAR images, while the metal ammo can is barely visible in the measurement data due to its location directly under an HVAC duct. As mentioned above, there was some uncertainty in matching the real position of the HVAC ducts in our CAD model, which explains slight misalignments between the two SAR images.

While the vertical walls positioned perpendicular to radar driving path does not appeared in the SAR image, scattering from the metal stud row (which is also aligned perpendicular to the radar driving path) is clearly visible in the simulated SAR image and also faintly appears in the measured data. In the inner court area, we observe the images of the 55 gallon drum and the large metal fuel tank. The ground bounce effect is the dominant factor in the scattering from the fuel tank. Notice the shadowing effect this fuel tank produces on the wall behind it. The cross-link part of the building was equipped with ceramic toilets and sinks, but these were not included in the model. However, we included the cinder block shower structure, cinder block dividing walls, and large metal electrical fixtures hanging from the ceiling (round 18" fluoresce light housing units, and metal conduits). Only the scattering from the first two long cinder block walls are visible in the image. Due to considerable field attenuation loss through these

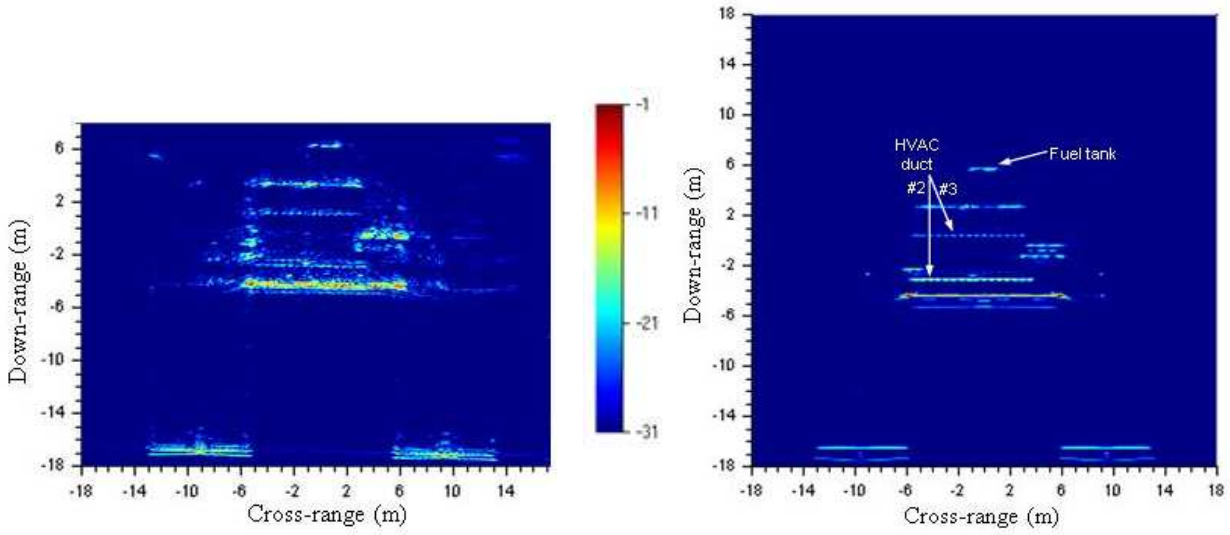

(a) (b)

Fig. 3. SAR images of the barrack building obtained along the radar path #2, showing (a) measured results and (b) simulated results.

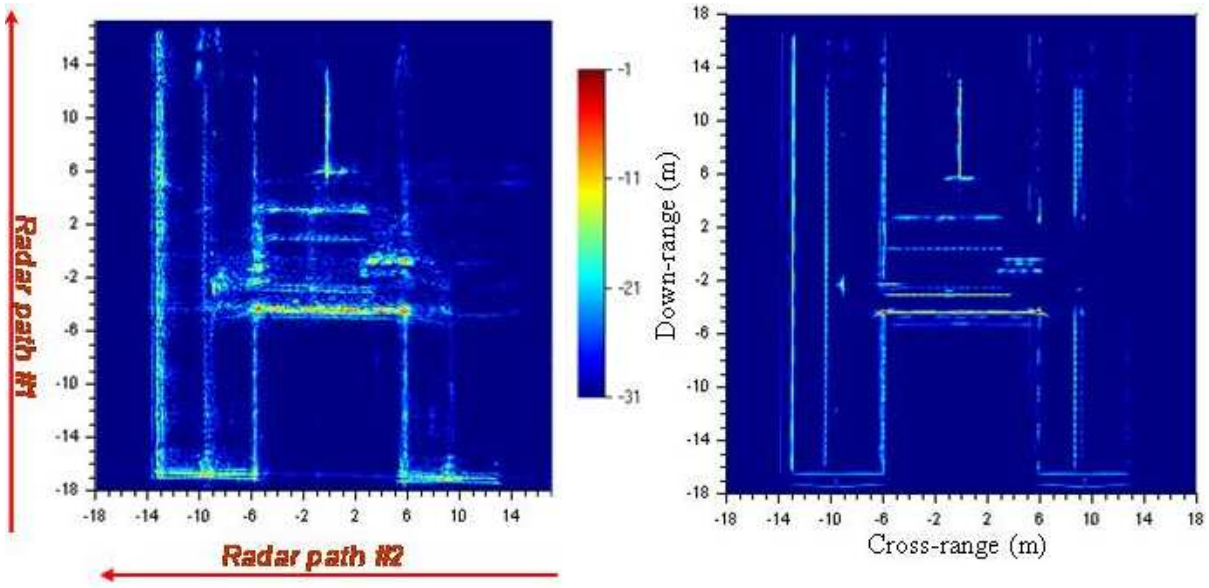

(a) (b)

Fig. 4. SAR images of the barrack obtained by combining the data along radar paths #1 and #2, showing (a) measured results and (b) simulated results.

cinder block walls, the objects directly behind do not appear in the image (these include the third cinder block wall, the shower structure, the large water heater tank in building #2, and a section of the back wall in building #2). Interestingly, we notice a pair of double parallel "zipper lines" in the vicinity of duct #5 location, connected by one faint line in the area behind the cross-link building. Similarly to the HVAC duct #1 image, the first bright line (closer to the radar) is due to the direct backscatter of HVAC duct #5, whereas the second line is due to multipath scattering. The weak intensity in the middle of the "zipper line" is due to the "blockage" effects of the wooden roof truss in the cross-link, which are now aligned mostly perpendicular to the radar line of sight. As for the measured SAR image, the HVAC duct #5 location is very close to the down range limit of our measurement

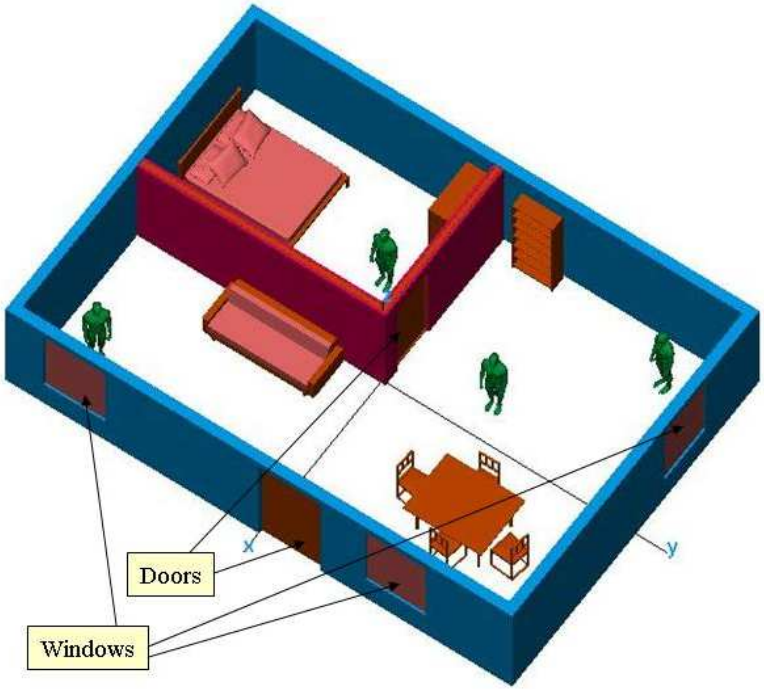

Fig. 5. The complex room mesh used in Section 4.2, containing humans and furniture objects (the ceiling and floor were removed in the figure).

setup. Thus, we can only notice a faint line at this location in the measured image.

Similarly to the images displayed in Fig. 2, Fig. 3 shows the SAR images obtained along the radar driving path #2. Again, the measured SAR image includes only part of the down-range building extent. In the simulated SAR images, the main contribution to the exterior walls return is from the ground bounce. In the cross link building, the scattering responses from the HVAC ducts #2 (located in the front, near the radar path) and duct #3 (located in the rear) display the same zipper line characteristic as seen in Fig. 2. Due to additional "blockage" of the wood beams in the roof truss from the radar view, the response from the HVAC duct #3 is weaker than that from the HVAC duct #2.

In Fig. 4 we computed the pixel-by-pixel incoherent sum of the two SAR images taken from the two sides of the building for both measured and simulated data as shown in Figs. 2 and 3. Fig. 4a shows the back-projected SAR image of the near-field data from the SIRE radar, with a constant 60^0 aperture window for every pixel. Again, notice that the measurement data does not cover the entire down-range extent of the building in either direction. Fig. 4b displays the simulated far-field spotlight SAR image, with a 20^0 effective aperture, and a depression angle of 11^0. Due to the different integration angle, we expect much better cross range resolution in the measurement image. Nevertheless, the agreement between the model and the measurement is very reasonable, with the modeled image displaying most of the major scattering centers. In both the simulated and measured SAR images, the strongest response is not coming from the long sides of the "H" (those walls being closest to the radar), but rather from the front wall in the cross-link building. This is the effect of the extra ground plane area in front of this wall, which effectively increases the wall's radar cross section (remember that the ground plane is finite in the Xpatch model, whereas in the measurement the antenna beam footprint on the ground is finite as well).

4.2. SAR images of a complex room based on FDTD models

In this section we present SAR images of a complex room (different from the building described in Section 4.1) obtained by FDTD simulations. The room is shown in Fig. 5. The exterior walls are made of 8" brick and are equipped with glass windows and a

wooden door. There is also an interior wall made of 2" thick sheetrock (equipped with a door as shown in the figure). The ceiling and floor are modeled as 2" thick concrete slabs. There are four humans in this mesh, placed at different azimuth orientation angles. We added the following furniture objects: a bed, a couch, a bookshelf, a dresser, and a table with four chairs. These objects are made primarily from wood (except for the mattress and cushions where we used some generic fabric material). The complex room overall dimensions are 10 m by 7 m by 2.2 m (197" by 138" by 87"). With an FDTD cell resolution of 1 cm, the overall grid size is 740 x 1050 x 270 cells. The frequency band extends from 1 to 2 GHz. For each image we use an aperture of 20° centered at broadside with respect to one side of the room. When the aperture center is along the *x* axis, looking from left to right, we obtain the image in Fig. 6a (V-V polarization). When the aperture center is along the *y* axis, looking from bottom to top, we obtain the

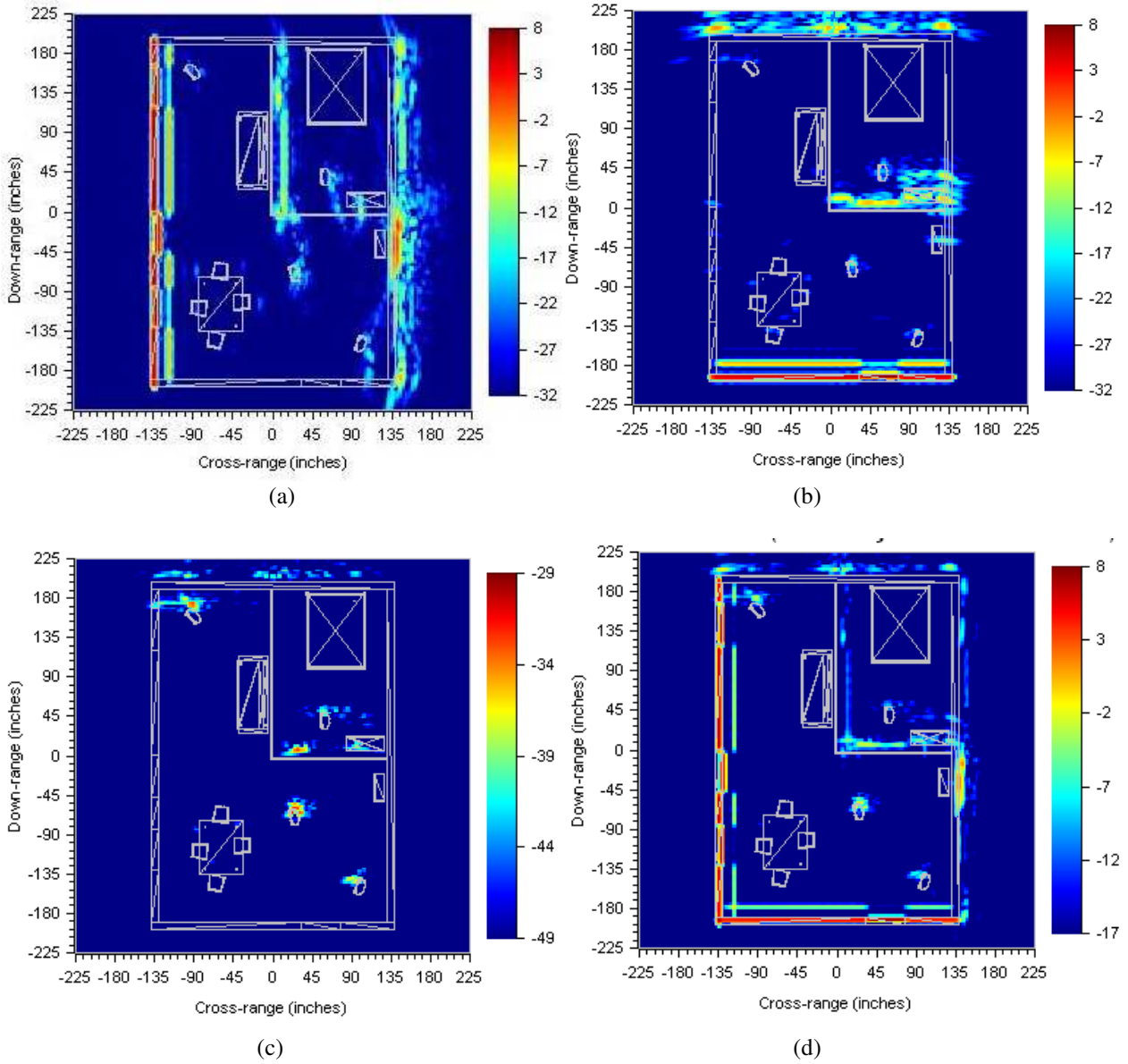

Fig. 6. SAR images of the complex room described in Fig. 5, for 1 GHz bandwidth centered at 1.5 GHz, 20^0 aperture, showing (a) V-V polarization, radar looks from left to right; (b) V-V polarization, radar looks from bottom to top; (c) V-H polarization, radar looks from bottom to top; (d) combination of the images (a) through (c).

images in Figs. 6b (V-V polarization) and 6c (H-V polarization). The walls perpendicular to the propagation direction in the aperture center are emphasized in the co-polarization images.

The humans can be distinguished fairly clearly in the images in Fig. 6. The human images are brighter when they are located directly behind a window or door. On the other hand, the furniture objects (which are made primarily of wood) do not contribute much to the images. An interesting effect is the human shadows projected onto the walls behind the humans (including the interior wall). A detailed explanation of this phenomenon was provided in Dogaru and Le, 2008b. For the cross-polarization image (Fig. 6c), we notice that only the humans have a significant contribution, together with their ghosts projected onto the walls. The explanation is that the cross-polarization fields reflected or diffracted from the planar faces, straight edges and corners of a room, as well as from regular-shaped furniture objects should be very small, unlike the return from the human body, which has an irregular shape. The image in Fig. 6c shows that using the cross-polarization mode can significantly reject the walls and other furniture objects from the SAR image. The images in Figs. 6a through c can be combined in various ways to enhance the overall image quality. Thus, by incoherently adding the images obtained in co-polarization and cross-polarization modes (after re-normalizing the dynamic ranges), we created the image in Fig. 6d that emphasizes both the building layout (as in co-polarization) and the human targets (as in cross-polarization).

5. CONCLUSIONS

The STTW radar technology has received considerable interest in the defense industry during the last few years. Several systems, mostly based on human motion detection, are already operational. However, the development of radar systems for building imaging is in a less advanced stage. ARL has demonstrated STTW imaging capabilities by reconfiguring its SIRE forward-looking radar to a side-looking operational mode. This paper describes the experimental setup and shows SAR images obtained through measurements. Moreover, we compared these images with those obtained through Xpatch computer simulations. Although there were several differences in the way the two sets of data were generated, the match is generally very good. In Section 4.1 we provided a detailed account of certain interesting features noticeable in the images. More details can be found in Le et al., 2008.

Another STTW-related research direction at ARL is investigating the phenomenology of operating an UWB imaging radar in such an environment through computer modeling. This allows us to understand some important phenomenological effects, as well as predict the performance and limitations of STTW radar systems. This paper presents large-scale simulations of a complex room achieved via the FDTD algorithm. One very interesting effect visible in the SAR images shown in Section 4.2 are "ghosts" of the targets projected onto the back walls. These "ghost" images can trigger false alarms, unless they are eliminated through some smart image processing algorithms. One should note that this issue is relevant to a Doppler or moving target indicator (MTI) radar that operates in a building environment as well. Another interesting idea is to operate the radar in cross-polarization mode, in order to reject the walls and many furniture objects, while emphasizing the human targets. However, these advantages come at the cost of a very low overall signal level, where the system noise may become a serious limiting factor. In general, combining images taken from different angles (sides of the building) and different polarizations can enhance the capabilities of a STTW radar system, and can produce the complete building layout, including the targets placed inside.

REFERENCES

Dogaru T. and Le C., 2008a: "Simulated radar range profiles of a simple room as computed by FDTD and Xpatch," ARL, Adelphi, MD, Technical Report ARL-TR-4420, Apr. 2008.

Dogaru T. and Le C., 2008b: "SAR images of rooms and buildings based on FDTD computer models," submitted to the *IEEE Transactions on Geoscience and Remote Sensing*, 2008.

Le C., Dogaru T., Nguyen L., and Ressler M., 2008: "UWB radar imaging of building interiors: measurements and predictions," submitted to the *IEEE Transactions on Geoscience and Remote Sensing*, 2008.

Nguyen L. and Sichina J., 2007: "SAR image formation using phase-history data from non-uniform aperture," *Proceedings of SPIE*, Vol. 6547, 2007.

Ressler M., Nguyen L., Koenig F., Wong D., and Smith G., 2007: "The ARL Synchronous Impulse Reconstruction (SIRE) forward-looking radar," *Proceedings of SPIE*, Vol. 6561, 2007.

Soumekh M., 1999: Synthetic Aperture Radar Signal Processing, John Wiley & Sons, 1999.

Taflove A., 1998: Advances in Computational Electrodynamics: The Finite-Difference Time-Domain Method, Artech, Norwood, MA, 1998.